DISK-RESOLVED VALIDATION OF A FRACTAL ROUGH THERMAL MODEL FOR THE MOON.
K. S. Wohlfarth[1], C. Wöhler[1], J. Helbert[2], H. Hiesinger[3], and the MERTIS Team, [1] Image Analysis Group, TU Dortmund University, Otto-Hahn-Str. 4, 44227 Dortmund, Germany (kay.wohlfarth@tu-dortmund.de), [2] Institute for Planetary Research, DLR, Rutherfordstr. 2, 12489 Berlin, Germany. [3] Institut für Planetologie, Wilhelm-Klemm-Str.10, 48149, Germany

Introduction: At the end of July 2018, the Chinese weather satellite 高分四号 (Gaofen-4) acquired disk-resolved images of the Moon for five different illumination geometries and at six bands in the VIS-NIR and MIR [1]. The MIR measurements are a valuable testbed for the fractal thermal roughness model implementation developed by the authors [2] and represent an occasion to apply a thermal model to an entire highly resolved planetary disk. Our study complements the disk-integrated validation of the standard thermal model by [3]. We find good agreement between our model and the new measurements. Fine-tuning the model yields a mean slope angle of $\bar{\theta}$=20.13° for highlands and $\bar{\theta}$=24.51° for maria.

Dataset and Methods: The dataset is comprehensively presented in [1] and supplementary material. For testing the thermal model, we use the only infrared channel of Gaofen-4 between 3.50–4.10 µm with a center wavelength of 3.77 µm and a ground resolution of ~4 km/pixel. We analyzed images captured in 2018 on 25th June, 28th June, and 30th June under phase angles of 30.01° (waxing moon), 3.88° (full moon), and 26.92° (waning moon). Our study takes three steps (I-III). *I Reflectance Removal:* The radiance at 3.77 µm is a superposition of ~10 % reflected solar radiation and ~90 % thermal emission. We apply the Hapke photometric model with b = 0.21, c = 0.7, and $\bar{\theta}$=11° from [4] and simulate the reflected radiance of the visible disk. We then subtract it from the radiance measurements such that only the thermal emission remains. Using spectra of lunar returned samples [5], we find a correlation of R=0.98 between the albedo at 2.5 µm and 3.77 µm. This allows a confident extrapolation of the single scattering albedo of M³-derived albedos to the Gaofen-4 MIR band around 3.77 µm. The opposition surge varies spatially and hence introduces a considerable amount of uncertainty. Consequently, we concentrate on the observations with phase angles of 30.01° and 26.92° degrees. *II Thermal Modeling:* Our thermal roughness model [2] partly builds upon [6], [7], [8], and [9] and outputs the thermally emitted radiance at 3.77 µm of the lunar disk as seen at a specific observation time. We perform a perspective projection of a lunar 3D model with topography [10]. This step yields the projected lunar disk for a specific observation time. The modeled disk is pixelated and each pixel is associated with an individual set of geometric input parameters, i.e., incidence angle i, emission angle e, and azimuth φ. We also project maps of the directional-hemispherical albedo A_{dh} and the emissivity ε. The map of A_{dh} was derived from M³ data [11, 8]. Because of the strong correlation (R = 0.98) between the albedo at 2.5 µm and 3.77 µm of the lunar returned samples, we compute the directional hemispherical reflectance r_{dh} at 3.77 µm from the M3 global mosaic. Therfore, we use the Hapke-parameters from [4] and derive the emissivity ε via Kirchhoffs law $\varepsilon = 1\text{-}r_{dh}$. Furthermore, we generate two fractal random rough 3D models of the regolith that are based on the statistical analysis of [12] with an average $\bar{\theta}$=20.13° and one with an average $\bar{\theta}$=26.40°. The 3D models consist of 300 x 300 pixels with 1 mm/pixel such that the resolution matches the scales that are isothermal on the Moon [13, 2]. For each pixel of the projected lunar disk, we take the input parameters i, e, φ, A_{dh}, and ε and compute the thermal emission of the two rough surface models with self-heating and shadowing according to [2]. Because many parameter sets are similar, we prune the parameter space to only 2% of the original points. Finally, we obtain the thermal emission that is associated with each pixel of the projected disk for two different roughness levels. *III Finetuning:* Because minor differences between individual instruments such as M³ and Gaofen-4 are commonly observed, we introduce a gain factor g that modulates the emissivity. We find that g = 0.96 generates the best matches by slightly lowering the whole radiance level. Because the exact roughness for the fractal roughness implementation is unknown in advance, and the roughness between maria and highlands may differ, we treat both regions individually. We find that the roughness for highlands is already well modeled by the fractal surface with $\bar{\theta}$=20.13°. For mare regions, a mixture of the radiance computed from both fractal surfaces yields reasonable results that correspond to a mean slope of $\bar{\theta}$=24.51°. These parameters generally align with [13], who reported an RMS slope of 20°-35°, and are slightly lower than those of [14], who find 30.17° for maria and 36.77° for highlands. More detailed analyses are necessary to improve the understanding of roughness variations.

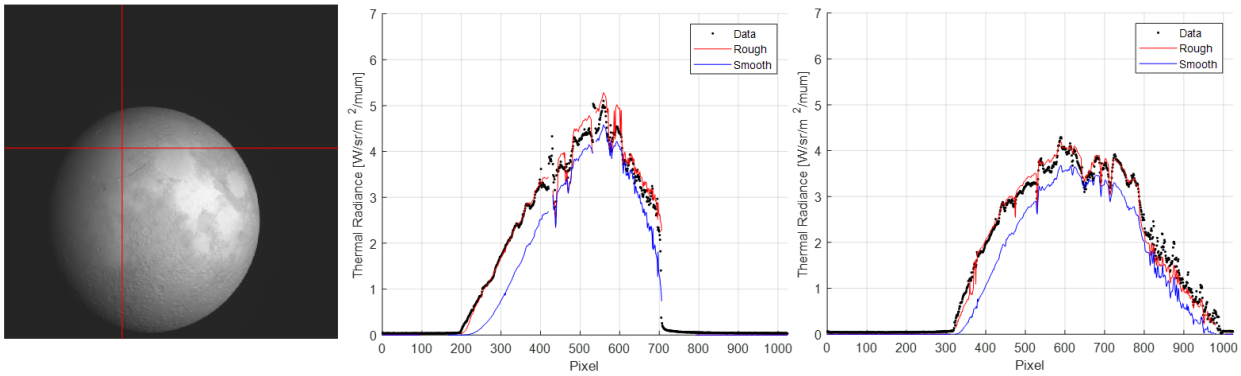

Figure 1: Left: Radiance on 25th July 2018 [1]. Middle: Thermal radiance along horizontal profile. Right: Thermal radiance along vertical profile. Note that mare regions appear brighter than highlands.

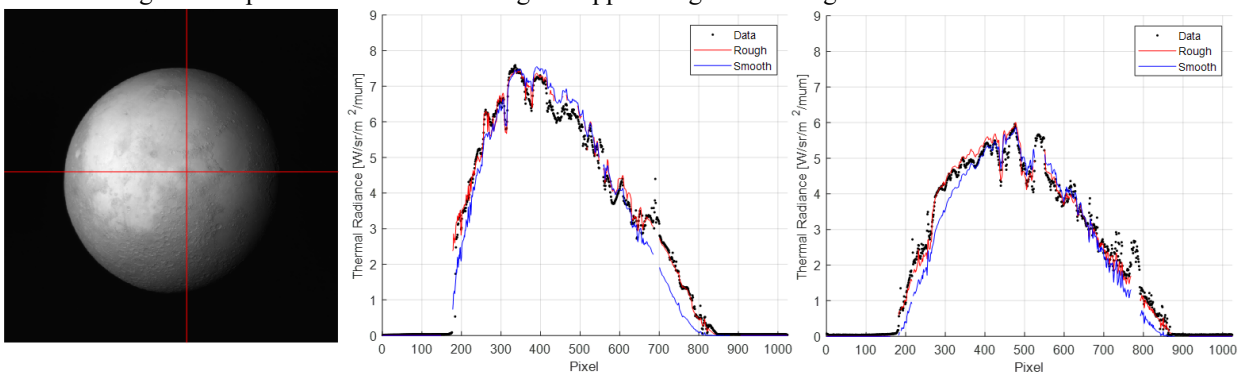

Figure 2: Left: Radiance on 30th July 2018 [1]. Middle: Thermal radiance along horizontal profile. Right: Thermal radiance along vertical profile.

Results: Figure 1 (left) shows the measured radiance on 25th July 2018. The thermal radiance of the horizontal profile and the vertical profile are shown in Figure 1 (middle) and (right), respectively. It is evident that the rough-surface thermal modeling results (red line) match the measurements (black dots): The curvature toward the limb and the terminator and the differences between mare and highland are well reproduced. Compared to the thermally emitted radiance of a smooth surface (blue line), it becomes clear that roughness is necessary to elevate the radiance at large incidence angles. Figure 2 (left) shows the measured radiance on 30th July 2018. Again, the modeled radiance of the horizontal profile (Figure 2 (middle)) and the vertical profile (Figure 2 (right)) are consistent with the measured thermal radiance. Overall, our thermal roughness model is well suited to simulate the thermal emission of the lunar surface.

Conclusion: These results demonstrate the capability of rough thermal models for disk resolved infrared imagery and support two recent studies of the authors. Firstly, the analysis of the 3 µm OH/H_2O absorption band on the Moon requires the removal of excess thermal radiation. Former studies [11, 8] employed a comparable thermal roughness model. Because the present study shows that the thermal model adequately captures the variations between different compositional regions and the global variations toward the limb at ~3.77 µm wavelength, we conclude that our former OH/H_2O studies [11, 8] mapped the true variations of hydroxyl across the lunar surface. Secondly, we use the thermal model to extract emissivity from spectral measurements of MERTIS onboard the BepiColombo spacecraft. We already applied the model to MERTIS lunar flyby data [2]. In the future, it will be used for the Mercury flyby in 2025 with albedo maps of Mercury and new roughness estimates. This study stresses the importance of an adequate albedo map and shows that our model is well suited for thermal modeling necessary for emissivity retrieval from MERTIS measurements.

References: [1] Wu, Y. et al. (2021) Geophysical Research Letters, 48, e2020GL088393. [2] Wohlfarth et al. (2021)) LPSC LII, abstract #2548. [3] Müller et al. (2021) A&A, 650, A38. [4] Warell, J. (2003) Icarus 167, 271-286. [5] Salisbury, J. (1997) Icarus 130, 125–139. [6]Davidsson, B.J. et al. (2015) Icarus, 252,1-21. [7] Rozitis, B. and Green, S. F. (2011) MNRAS 415(3), 2042-2062. [8] Grumpe, A. et al. (2019) Icarus 321,486-507. [9] Shkuratov et al. (2011) PSS, 59(13), 1326-1371.[10] Barker, M. K. et al. (2016) Icarus 273, 346-355. [11] Wöhler C. et al. (2017) *Sci. Adv.*, 3(9). [12] Helfenstein, P. and Shepard, M. K. (1999) Icarus 141 (1), 107- 31. [13] Bandfield, J. L. et al. (2015) Icarus 248, 357-372. [14] Rubanenko, L. (2020) JGR Planets, 125, e2020JE006377.